Coincidence measurements of highly charged ions interacting with a clean Au(111) surface

C. Lemell,[1,2,*] J. Stöckl,[1] J. Burgdörfer,[2] G. Betz,[1] HP. Winter,[1] and F. Aumayr[1]
[1]*Institut für Allgemeine Physik, TU Wien, Wiedner Hauptstraße 8-10, A-1040 Vienna, Austria*
[2] *Institute for Theoretical Physics, Vienna University of Technology, Wiedner Hauptstraße 8-10, A-1040 Vienna, Austria*
(Received 6 July 1999; revised manuscript received 1 September 1999; published 10 December 1999)

We have measured electron number statistics of highly charged ions interacting with a clean single crystal Au(111) surface under various angles of incidence in the range from 45° to almost 0° with respect to the surface. For small angles of incidence (typically about 3°) we have also measured the scattering distribution of the reflected projectiles on a position-sensitive detector in coincidence with the number of emitted electrons. Our results allow a clear separation of above- and below-surface electron emission. By comparison with electron emission yields for very slow projectiles under normal incidence conditions, we are able to determine the number of electrons produced by potential and kinetic emission processes. Simulations of the kinetic electron emission along specific trajectories (e.g., projectiles reflected from ideally flat surface areas as opposed to those entering the crystal at target imperfections) show good agreement with our experimental results.

PACS number(s): 79.20.Rf, 61.85.+p, 79.60.Bm

I. INTRODUCTION

Since the 1950s, when Hagstrum first performed experiments on ion-surface interaction using low-charge state ions [1], new powerful ion sources as well as improved experimental techniques have strongly developed this field of research. Nowadays, various secondary particles (photons, electrons, sputtered target atoms) produced in highly charged ion (HCI) surface interactions are detected with dramatically improved resolution (for an extensive review see, e.g., [2], and references therein). Available projectile charge states q range from 1 to 92 (bare U ions), as target materials solids from low work function metals (e.g., Cs) to large band-gap insulators (e.g., LiF) are used.

These experiments support the picture of the so-called ''hollow-atom'' formation, a highly excited transient projectile state that decays to the ground state via emission of electrons and photons [3,4]. Until now, most of the experiments dealt with just one aspect of the interactions (e.g., total electron yields [5,6], x-ray emission [7], energy distribution of emitted electrons [8–10], target sputtering [11–13], image-charge acceleration [14–16]). Recently, Morosov *et al.* performed an experiment measuring the charge state and distribution of scattered projectiles in coincidence with the angular, energy, and number distribution of electrons emitted into the half-sphere above the target using a multicoincidence technique [17]. Such coincidence experiments (''experiments of the second generation'') have the potential to allow deeper insight into the processes involved in ion-surface interaction.

In recent years we have developed a sophisticated experimental technique to measure the electron-emission statistics (EES) for HCI impinging vertically on clean polycrystalline metal [6,18] and insulator surfaces [19]. In this paper we primarily investigate grazing-incidence angles at a monocrystalline target surface and record the impact position of scattered projectiles on a two-dimensional (2D) position-sensitive detector in concidence with the number of emitted electrons. The main purpose of these studies is to connect different electron-emission characteristics with specific classes of trajectories. In a further step, we want to relate the number of electrons to the energy loss of the primary particle.

Section II gives a short description of our experimental setup followed by the experimental results in Sec. III. The presentation of a theoretical model aimed at describing our findings concludes our paper (Sec. IV). First results have already been presented in Ref. [20].

II. EXPERIMENTAL SETUP

Our experimental setup is served by the 5-GHz ECR-ion source at TU Wien [21], which provides multiply charged ions (for this series of experiments Ar^{q+}, $q \leqslant 9$; O^{q+}, $q \leqslant 7$; N^{q+}, $q \leqslant 6$) with kinetic energies between 1 and $10q$ keV. The extracted ions are mass-to-charge separated, collimated, and transported to a UHV scattering chamber (base pressure $p \simeq 10^{-10}$ mbar).

The ion beam is directed onto a Au(111) surface that has been prepared by cycles of sputtering and annealing [22]. The angle of incidence ψ can be varied between $0°$ and $90°$. Under grazing-incidence conditions the angular distribution of scattered particles, as well as parts of the beam passing above the target without interaction, are recorded on a 2D position-sensitive detector (PSD). Electrons produced during ion-surface interaction are extracted by a weak electric field and focused onto a surface barrier detector biased at $+25$ kV. The number of electrons emitted in a particular scattering event is determined from the pulse height of the electron detector. The electron yield (i.e., the mean number of electrons emitted per ion impact) is determined from the electron-emission statistics [18]. The influence of the electric extraction field on the ion trajectories has been taken into account in our data evaluation procedure. Signals from both detectors are recorded either in coincidence (synchronized in time and stored as n-tuples) or in noncoincidence mode (for

*Author to whom correspondence should be addressed. Electronic address: lemell@concord.itp.tuwien.ac.at

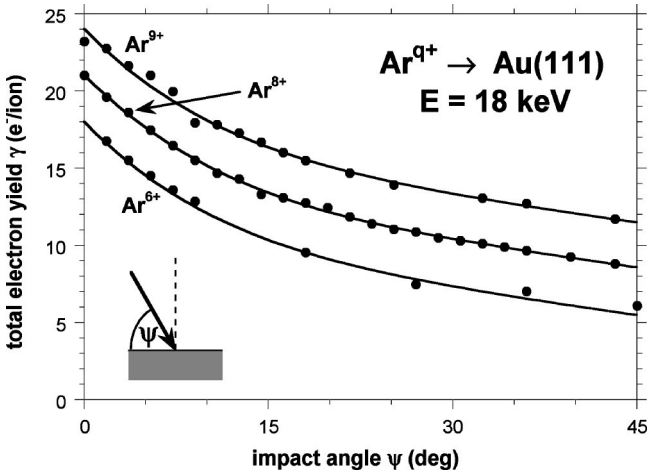

FIG. 1. Angular-dependent measurement of γ for 18-keV $Ar^{q+}(q=6,8,9)$ on Au(111).

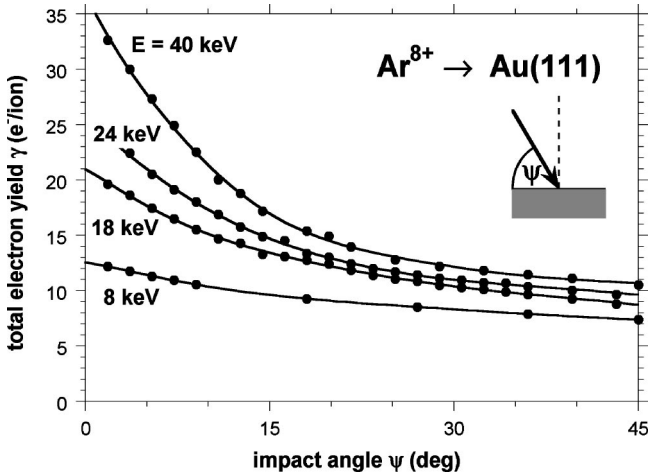

FIG. 2. Angular-dependent measurement of γ for 8-, 18-, 24-, and 40-keV Ar^{8+} on Au(111).

incidence angles $\psi \geqslant 10°$ when measuring electron emission only). A detailed description also containing a schematic drawing of this experimental setup can be found in Ref. [23].

III. EXPERIMENTAL RESULTS

In the first part of this section we present results of angular-dependent electron-yield measurements and describe information that can be extracted from these data. In the second subsection we concentrate on results of coincidence measurements between scattered ions and emitted electrons in glancing-angle-scattering geometry and their interpretation.

A. Angular-dependent electron yield

It is well known that above the threshold velocity for kinetic electron emission (KE) the electron yield γ shows a strong dependence on the projectile angle of incidence ψ [24]. For smaller angles of incidence the bulk of electrons emitted along the trajectory within the solid has a comparably larger escape probability. To first approximation a $1/\sin\psi$ dependence of γ can be expected. In our experiment we find deviations from a $1/\sin\psi$ fit only for small and large angles of incidence. The latter can be explained by our experimental setup that has been optimized for small ψ and does not have a 100% electron collection efficiency for $\psi > 45°$, whereas the reason for the deviation for $\psi < 10°$ is the increasing number of reflected projectiles. Such projectiles produce less electrons along their trajectory (see Sec. III B) and consequently show a reduced mean electron yield γ (see also below). Lines connecting data points in Figs. 1 and 2 are therefore not $1/\sin\psi$ fits but only meant to guide the eye.

In Fig. 1 we show results of impact-angle-dependent measurements of γ for different charge states of Ar directed onto a clean Au(111) surface. The experiments have been performed for Ar^{6+} ($E_{pot} \simeq 310$ eV), Ar^{8+} ($E_{pot} \simeq 580$ eV), and Ar^{9+} ($E_{pot} \simeq 975$ eV), each with a kinetic energy of 18 keV, for which the velocity of the projectiles is about twice the threshold velocity for KE [25]. It can be seen that all three data sets show the expected increase in γ toward smaller angles of incidence. Although Ar^{9+} has an *L*-shell hole that could give rise to increased subsurface potential electron emission (PE) and, accordingly, to a different angular dependence, the curves are almost parallel over the whole range of ψ. We therefore conclude that KE dominates the impact-angle-dependent part of γ for all charge states.

This interpretation is further supported by results on the angular dependence of the electron yield for a single charge state (Ar^{8+}) with kinetic energies ranging from 8 to 40 keV (Fig. 2). While for $E_{kin} = 8$ keV ($\sim 2 \times 10^5$ m/s) we observe only a 40% increase in γ relative to the value for large angles, the amount of emitted electrons is three times larger for $E_{kin} = 40$ keV ($\sim 4.4 \times 10^5$ m/s). In order to determine an approximate value of the threshold velocity for KE, we plot the electron yield for different values of ψ over the velocity of the projectiles (Fig. 3). All four lines intersect at $8.5 e^-$/ion and a velocity of about 1.6×10^5 m/s (~ 5.4 keV), which is in reasonable agreement with previ-

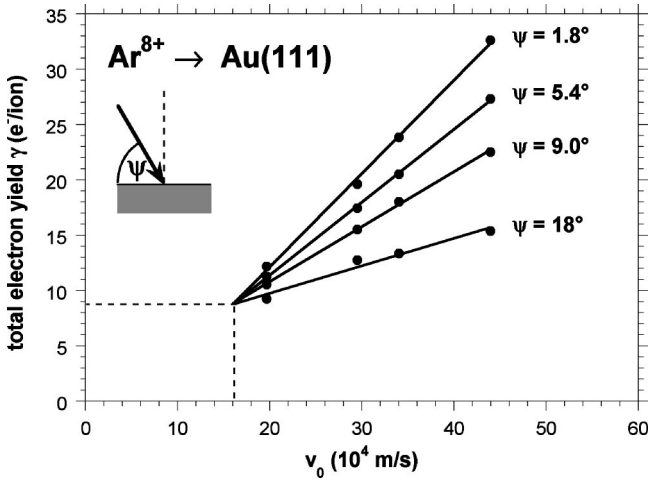

FIG. 3. Electron yield γ as a function of the ion velocity for specific angles of incidence ψ. The linear fits cross in one point defining an approximate value for the threshold velocity of KE.

ous results on KE from clean polycrystalline gold by Eder *et al.* [25].

B. Coincidence measurements

To perform coincidence measurements, the signals from the EES and PSD detectors were amplified, delayed in time, and fed into a multiparameter analog-to-digital converter. The gate signal was provided either by the EES or the PSD branch of these electronics to allow measurement of both coincident as well as noncoincident events. With the help of this additional information a separation of the contributions from PE and KE from above and below the target surface could be achieved. As one example for a whole series of measurements with Ar^{q+}, N^{q+}, and O^{q+} ions, we discuss data for 18-keV Ar^{8+} ions impinging on a clean Au(111) surface at an angle of incidence $\psi = 5°$ ($E_\perp = 136$ eV, $v_\perp \approx 2.5\times 10^4$ m/s). Apart from the signature of the direct beam that is recorded on the PSD only due to random coincidences with field-emission electrons, we observe a broad structure (FWHM$\simeq 5°$) with its maximum at a scattering angle $\theta = 10°$ (specular reflection). Scattered projectiles were detected up to the edge of our PSD. The comparably large width of the scattering distribution indicates that our target is not perfectly flat [26]. Due to the coincident detection of electrons and ions, the imperfections do not provide a major obstacle as different trajectories can be analyzed separately.

At the same position as the maximum of the scattering distribution (specularly reflected projectiles) we observe a local minimum of the electron yield γ [see inset in Fig. 4(b)]. In the outer area of the distribution (edges of PSD) γ is by at least a factor 2 higher than in the center. This will be discussed in more detail with the coincident EES spectra for different regions of the PSD. In Fig. 4(a) we compare the total ES spectrum (electron signals measured noncoincidently) with its coincidence parts. The total spectrum consists of at least three contributions. The first one at small electron numbers ($\leqslant 3e^-$/ion) results mainly from field emission and can be easily subtracted. The second part peaks at about $8e^-$/ion and also appears in the coincidence spectrum. The third group has a broad maximum at about $20e^-$/ion and is strongly reduced for measurements in coincidence with scattered particles. This missing part of our total EES spectrum [difference spectrum in Fig. 4(a)] can be attributed to electron production along projectile trajectories of type 3 [see inset in Fig. 4(a)] which end inside the bulk or at scattering angles too large to be detected by our PSD.

With the help of EES spectra measured in coincidence with projectiles hitting specific areas of the PSD, we can separate different parts of the coincidence spectrum [Fig. 4(b)]. The ES spectrum labeled 1 has been taken for the central area of the projectile scattering distribution (see inset), spectrum 2 for its outer parts. Spectrum 1 can be associated with projectiles that have been specularly scattered at the surface [trajectory 1 in Fig. 4(a)], whereas projectile trajectories ending up in the outer regions of the PSD entered the target at surface imperfections and left it after having

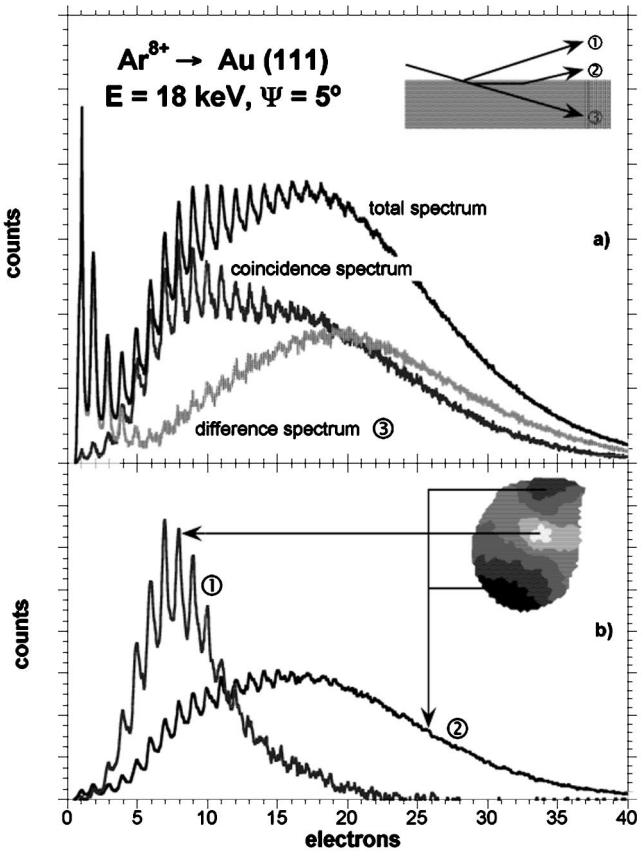

FIG. 4. Electron emission statistics spectra for 18-keV Ar^{8+} ions impinging on a clean Au(111) surface. (a) total and coincidence EES spectra; (b) spectra from specific regions of the PSD.

undergone multiple scattering below the topmost atomic layer, causing exit angles slightly different from ψ [trajectory 2 in Fig. 4(a)]. The long tail of the distribution appearing towards higher electron multiplicities in spectrum 1 can be explained by projectiles with trajectories of type 2 that end up ''accidentally'' (due to multiple scattering) in the central area of the scattering distribution. Further justification of our separation procedure comes from projectile time-of-flight spectra recorded in coincidence with the signals from EES and PSD detectors [23] that show an increased energy loss for projectiles of type 2 as compared to those scattered specularly (type 1).

The difference between ES spectra 1 and 2 can be attributed to processes taking place below the topmost atomic layer. To determine the contributions of PE and KE to the above-surface yield we compare spectrum 1 with results of earlier experiments by Kurz *et al.* [27], which have been conducted for a polycrystalline Au surface under normal incidence conditions with a similar total projectile energy as our energy component normal to the surface (130 eV as compared to 136 eV including image-charge acceleration). For such slow projectiles penetration below the first target layer and kinetic electron emission can be ruled out. We find almost identical EES spectra with a slightly higher electron yield ($\Delta\gamma \simeq 1e^-$ from KE) for the grazingly incident Ar^{8+}

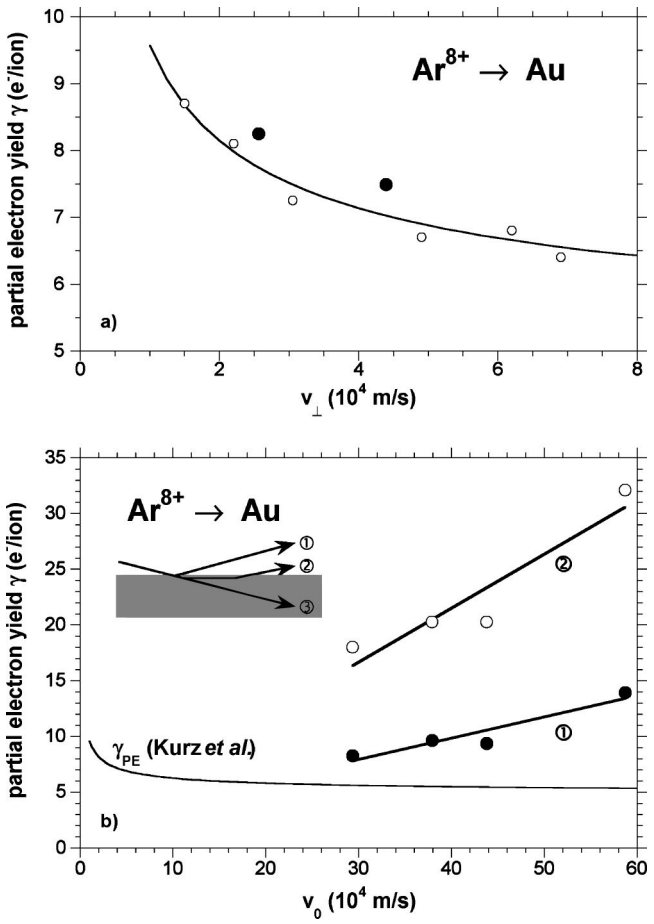

FIG. 5. (a) Comparison of electron yields γ measured for fast-grazing and slow normal-incident Ar^{8+} ions on Au plotted vs $v_\perp$. Full symbols correspond to 18-keV projectiles, open symbols to data from Kurz *et al.* [27]. (b) Electron yields for trajectories of type 1 and 2 (see inset) vs v_0 (all projectiles have identical $v_\perp$) compared to PE as measured by Kurz *et al.* [27].

projectiles. For 136-eV Ar^{8+} ions impinging on a Au surface we performed calculations based on the classical-over-the-barrier (COB) model (only PE [3]) and weighted the result with theoretical detection probabilities for emitted electrons [28]. The simulation gives a yield of $6.5e^-$/ion, which is very close to the experimental value of $\gamma = 7.1e^-$/ion. This supports our identification of spectrum 1 as predominant above surface PE with almost negligible KE contributions.

For different projectile/target combinations and different projectile energies similar results were found. Figure 5(a) shows electron yields of Ar^{8+} ions scattered under specular reflection conditions off a Au(111) surface with an energy of 18 keV as a function of the velocity component normal to the surface $v_\perp$. Full symbols denote our experimental results, open symbols represent data of Kurz *et al.* [27] together with a fitting curve ($\gamma_{PE} = c_1 + c_2/\sqrt{v}$), which defines the lower bound for our electron yields. Since Kurz *et al.* used normally incident ions with a velocity far too small to cause KE, the difference between their data and our results most likely comes from KE above the topmost atomic layer.

In Fig. 5(b) we plot measured yields for trajectories 1 and 2 (cf. inset) as a function of the initial projectile velocity. In

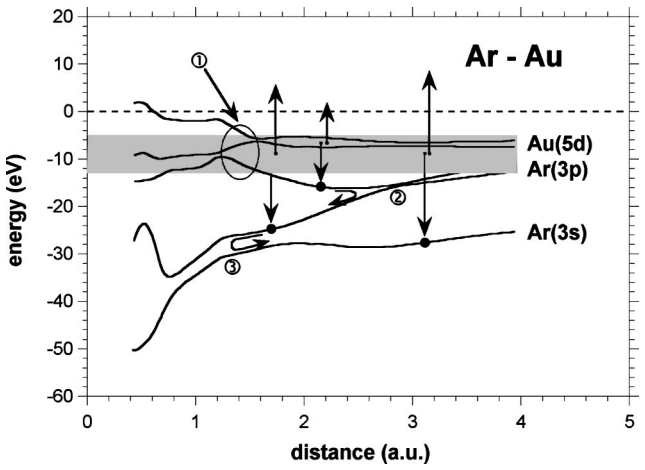

FIG. 6. Schematic drawing of processes entering our simulation. Electrons can be produced either by direct-impact ionization (1) or via holes created in the Ar $3p$ level (full circles) that can be transferred to lower-lying states at crossings 2 and 3 and filled by Auger-type processes.

all cases the velocity component normal to the surface was $v_\perp \simeq 3\times 10^4$ m/s. The curve at the bottom shows again γ_{PE} as fitted by Kurz *et al.* The difference between full and open symbols denoting the yield associated with trajectories of types 1 and 2, respectively, can be attributed to below-surface KE. It increases from about $10e^-$/ion for 18-keV particles to almost $20e^-$/ion in the case of 72-keV projectiles. The origin of these additional electrons will be explained in the following section.

IV. THEORETICAL DESCRIPTION

In order to explain the large difference in γ for specularly reflected projectiles and those entering the target, we performed Monte Carlo calculations for the kinetic emission for these classes of trajectories. It is assumed that in all cases the above-surface electron emission part due to potential emission ($\sim 7e^-$/ion; see discussion of our experimental results in Sec. III B) is the same and has to be added to our calculated KE electron yields to fit the data presented in Fig. 4. We started our calculations with projectiles in their ground state. As can be seen from Fig. 1 different initial projectile-charge states do not lead to changes in the angular dependence of the total electron yield indicating that the neutralization sequence is finished within a few a.u. after impact on the target surface. Since our calculations (see below) indicate path lengths of more than 100 a.u. within the solid for trajectories of type 2 we do not expect the initial projectile-charge state to be of major importance for the kinetic electron emission.

Two different processes entered our simulation (cf. Fig. 6). In the first one, target electrons are emitted by ''direct'' impact ionization in close projectile-target collisions. Impact ionization is expected to take place in collisions with impact parameters $b \leqslant 1.4$ (indicated by the arrow labeled 1 in Fig. 6), which is close to the mean radius of the $5d$ state in Au. In the second one, holes in projectile levels are created and refilled by Auger decay with both active electrons coming

from the conduction band of the target. The sequence ending with Auger emission from the conduction band starts with the creation of a hole in a bound state of the projectile. As the distance to the nearest target atom changes repeatedly along the trajectory, the hole can be transferred to deeper-lying levels when it passes avoided crossings appearing in the molecular-orbital (MO) diagram of Ar on Au [29]. For our simulations energy levels of Ar in the diagram have been corrected to fit results of density-functional calculations for Ar in Au. Electron-hole pair production in the conduction band of Au could be ruled out as an additional source of electron emission [30].

To determine the total kinetic emission yield due to these processes we summed their contributions over trajectories resulting from molecular-dynamics simulations [31]. The Ziegler-Biersack-Littmark potential [32] was used to calculate projectile-target atom scattering, interatomic interaction in the crystal was simulated using a tight-binding potential with a cutoff length of 6 Å. The target crystal had an initial temperature of 300 K. 18-keV Ar atoms were directed on a Au(111) target with different surface structures (ideal surface, steps, defects) under grazing angles of incidence and randomly varying impact positions. We approximated impact ionization per scattering event by

$$Y(b) = Y_0 \exp(-b/b_c). \tag{1}$$

Y_0 describes the probability for an electron to escape the solid, b_c is the range of the interaction. In our calculations we used $Y_0 = 0.4$ and $b_c = 1.3$ a.u. Both parameters can be estimated as follows: In every close projectile-target atom collision typically one electron is emitted in a binary-encounter-type process. This electron liberated close to the first atomic layer has an escape probability into vacuum close to 50%. From calculations of detection rates for low-energy electrons emitted at the surface [28], it is known that an escape probability and, hence Y_0 between 0.3 and 0.4 depending on the energy of the electron, would be correct. Since we did not simulate the energy distribution of the emitted electrons we chose a constant value of $Y_0 = 0.4$ assuming an initial kinetic energy of some 10 eV. The value for $b_c = 1.3$ a.u. has been chosen to be slightly smaller than the mean radius of the $5d$-state of Au ($\langle r \rangle_{5d} \simeq 1.4$ a.u.) based on the assumption that mainly electrons from this level are involved in the emission. Moreover, molecular-orbital calculations for gas-phase collisions show an avoided crossing of Au and Ar levels (cf. also Fig. 6) at an internuclear distance of 1.2 a.u. indicating that, apart from direct excitation in projectile-electron interactions, also MO-promotion processes could contribute to KE. From our calculations we find that the simple collisional KE process alone does not suffice to explain the high number of kinetically emitted electrons.

In our simulation additional electrons come from hole formation and filling at and below the surface. Based on the observation that for effective electron densities used to simulate Au in a local density-functional approach ($r_s \simeq 1.5$ a.u.) the $3p$ level of Ar lies close to the lower edge of the conduction band, we simulated a scenario for density-dependent hole creation. The $3p$ level was assumed to be

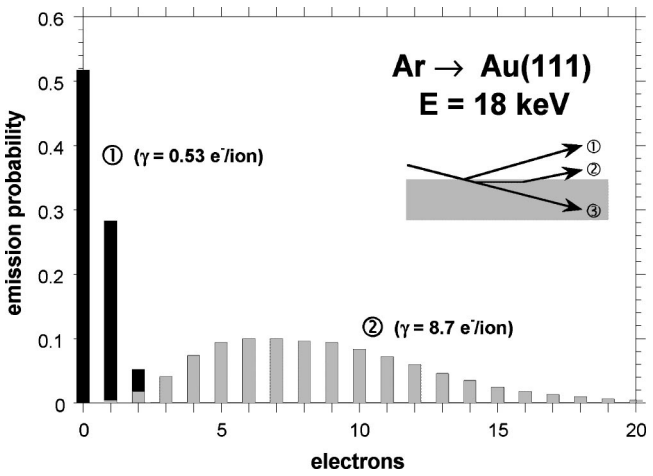

FIG. 7. Calculated kinetic electron-emission statistics. Black bars show KE for specular reflection, gray bars for projectiles entering the target (see insets).

atomic for densities $r_s > 1.5$ a.u. For close collisions with target atoms where the local electron density is enhanced (reduced r_s) it is immersed into the conduction band because of increased screening. Since the impact-angle-dependent part of the total electron yield does not depend on the initial charge state of the projectile (see Fig. 1) and calculations of highly charged ions interacting with metal targets showed an almost immediate relaxation of the projectile upon close impact on the surface [33], we start the collision sequence with the projectile in its ground state. Following each close encounter with an Au core we assigned the $3p$ level a probability to have ''captured'' a hole when becoming atomic after a collision. This probability was calculated from the resonant transfer rates used in the COB model [3].

Based on MO diagrams we calculated the probability for hole transfer to lower-lying states of the projectile. Candidates for such level-crossing regions of the Landau-Zener-Stückelberg- and Rosen-Zener-type can be found in Fig. 6 near 3 a.u. (marked by 2) and near 1.4 a.u. (marked by 3), respectively. A hole in a bound state of the projectile could be filled by an Auger process with both active electrons coming from the top of the conduction band (cf. Fig. 6). The rates for this process have been taken from Refs. [34,35]. The number of holes in a projectile was constrained to one at any time. The escape probability of the ejected electron was set to 0.4 ($E_{kin} \geqslant 10$ eV) as for electrons emitted via impact ionization.

Our results show dramatic differences in width and mean value between the two distributions for trajectories of type 1 and 2 (Fig. 7). Projectiles scattered specularly off the surface (full bars) produce about $1e^-$/ion. Projectiles that have entered the target at a step and undergo channeling (mainly between the first and second atomic layers, shaded bars) lead to the emission of a larger number of electrons ($\gamma_{KE} \simeq 9e^-$/ion). These findings are in good agreement with our experimental results [cf. difference between ES spectra 1 and 2 in Fig. 4(b)]. The impact-ionization process contributes to γ_{KE} with about seven electrons, while Auger decays produce only a minor fraction of KE ($\gamma_{Auger} \simeq 2e^-$/ion). The main

source of uncertainty in our calculation is the only moderately adapted (slightly shifted binding energies) MO diagram used to simulate hole creation in projectile-target interaction. It has been calculated for atomic collisions and could change considerably for the case of a crystal. However, since the contribution from the hole-creation- and filling process is comparably small, we do not expect improved MO diagrams to change our results significantly.

V. CONCLUSION

We have presented experimental investigations that give the possibility to separate above- and below-surface contributions to the total electron yield resulting from highly charged ions interacting with a single-crystal target. For specularly reflected projectiles we could determine the amount of electrons coming from potential and kinetic emission. We have shown that in our range of projectile velocities potential electron emission depends only on the impact velocity component normal to the surface $v_\perp$. Furthermore, we find kinetic electron emission to be strongly increased for projectiles undergoing multiple scattering after entering the target at surface imperfections even for relatively low velocities. With a simple model we were able to reproduce the difference between kinetic emission for surface channeled projectiles and those entering the target and undergoing multiple scattering with target atoms. It is shown that the main contribution to the kinetic emission yield comes from ionizing collisions with an impact parameter range $b \simeq 1.3$ a.u., which is close to the mean radius of the $5d$ state of Au. As an additional yet less important source of electrons we identified hole creation and filling in the projectile near the target surface. These two contributions together account for an electron-emission statistics similar in mean value and width to those measured in our experiment.

ACKNOWLEDGMENTS

We thank A. Arnau, I. Juaristi, and P.M. Echenique for help with density-functional calculations and valuable discussions on the theoretical aspects of our work, and P. Kürpick for giving us access to unpublished results. Our studies have been supported by Austrian Fonds zur Förderung der Wissenschaftlichen Forschung.

[1] H. D. Hagstrum, Phys. Rev. **96**, 325 (1954); **96**, 336 (1954).
[2] A. Arnau, F. Aumayr, P. M. Echenique, M. Grether, W. Heiland, J. Limburg, R. Morgenstern, P. Roncin, S. Schippers, R. Schuch, N. Stolterfoht, P. Varga, T. J. M. Zouros, and HP. Winter, Surf. Sci. Rep. **27**, 113 (1997).
[3] J. Burgdörfer, P. Lerner, and F. W. Meyer, Phys. Rev. A **44**, 5674 (1991).
[4] HP. Winter and F. Aumayr, J. Phys. B: At. Mol. Opt. Phys. **32**, R39 (1999).
[5] I. G. Hughes, J. Burgdörfer, L. Folkerts, C. C. Havener, S. H. Overbury, M. T. Robinson, D. M. Zehner, P. A. Zeijlmans van Emmichoven, and F. W. Meyer, Phys. Rev. Lett. **71**, 291 (1993).
[6] H. Kurz, K. Töglhofer, HP. Winter, F. Aumayr, and R. Mann, Phys. Rev. Lett. **69**, 1140 (1992).
[7] J. P. Briand, L. de Billy, P. Charles, S. Essabaa, P. Briand, R. Geller, J. P. Desclaux, S. Bliman, and C. Ristori, Phys. Rev. Lett. **65**, 159 (1990).
[8] J. Limburg, J. Das, S. Schippers, R. Hoekstra, and R. Morgenstern, Surf. Sci. **313**, 355 (1994).
[9] F. W. Meyer, S. H. Overbury, C. C. Havener, P. A. Zeijlmans van Emmichoven, J. Burgdörfer, and D. M. Zehner, Phys. Rev. A **44**, 7214 (1991).
[10] D. Niemann, M. Grether, A. Spieler, N. Stolterfoht, C. Lemell, F. Aumayr, and HP. Winter, Phys. Rev. A **56**, 4774 (1997).
[11] T. Schenkel, A. V. Barnes, A. V. Hamza, D. H. Schneider, J. C. Banks, and B. L. Doyle, Phys. Rev. Lett. **80**, 4325 (1998).
[12] T. Neidhart, F. Pichler, F. Aumayr, HP. Winter, M. Schmid, and P. Varga, Phys. Rev. Lett. **74**, 5280 (1995).
[13] M. Sporn, G. Libiseller, T. Neidhart, M. Schmid, F. Aumayr, HP. Winter, P. Varga, M. Grether, and N. Stolterfoht, Phys. Rev. Lett. **79**, 945 (1997).
[14] H. Winter, Europhys. Lett. **18**, 207 (1992).
[15] F. Aumayr, H. Kurz, D. Schneider, M. A. Briere, J. McDonald, C. Cunningham, and HP. Winter, Phys. Rev. Lett. **71**, 1943 (1993).
[16] F. W. Meyer, L. Folkerts, H. O. Folkerts, and S. Schippers, Nucl. Instrum. Methods Phys. Res. B **98**, 441 (1995).
[17] V. A. Morosov, A. Kalinin, Z. Szilagyi, M. Barat, and P. Roncin, Rev. Sci. Instrum. **67**, 2163 (1996).
[18] G. Lakits, F. Aumayr, and HP. Winter, Rev. Sci. Instrum. **60**, 3151 (1989); F. Aumayr, G. Lakits, and HP. Winter, Appl. Surf. Sci. **47**, 139 (1991).
[19] M. Vana, F. Aumayr, P. Varga, and HP. Winter, Europhys. Lett. **29**, 55 (1995).
[20] C. Lemell, J. Stöckl, J. Burgdörfer, G. Betz, HP. Winter, and F. Aumayr, Phys. Rev. Lett. **81**, 1965 (1998).
[21] M. Leitner, D. Wutte, J. Brandstötter, F. Aumayr, and HP. Winter, Rev. Sci. Instrum. **65**, 1091 (1994).
[22] H. Winter, C. Auth, R. Schuch, and E. Beebe, Phys. Rev. Lett. **71**, 1939 (1993).
[23] C. Lemell, J. Stöckl, HP. Winter, and F. Aumayr, Rev. Sci. Instrum. **70**, 1653 (1999).
[24] R. A. Baragiola, E. V. Alonso, and A. Oliva-Florio, Phys. Rev. B **19**, 121 (1979).
[25] H. Eder, M. Vana, F. Aumayr, and HP. Winter, Rev. Sci. Instrum. **68**, 165 (1997).
[26] R. Pfandzelter, Phys. Rev. B **57**, 15 496 (1998).
[27] H. Kurz, F. Aumayr, C. Lemell, K. Töglhofer, and HP. Winter, Phys. Rev. A **48**, 2182 (1993).
[28] C. Lemell, HP. Winter, F. Aumayr, J. Burgdörfer, and C. Reinhold, Nucl. Instrum. Methods Phys. Res. B **102**, 33 (1995).

[29] P. Kürpick (private communication).
[30] J. I. Juaristi, M. Rösler, F. J. Garcia de Abajo, H. Kerkov, and R. Stolle, Nucl. Instrum. Methods Phys. Res. B **135**, 487 (1998); (private communication).
[31] G. Betz and W. Husinsky, Nucl. Instrum. Methods Phys. Res. B **102**, 281 (1995).
[32] J. F. Ziegler, J. P. Biersack, and U. Littmark, in *The Stopping and Range of Ions in Solids*, edited by J. F. Ziegler (Pergamon, Oxford, 1985).
[33] J. Burgdörfer, C .O. Reinhold, and F. W. Meyer, Nucl. Instrum. Methods Phys. Res. B **98**, 415 (1995).
[34] A. Arnau, R. Köhrbrück, M. Grether, A. Spieler, and N. Stolterfoht, Phys. Rev. A **51**, R3399 (1995).
[35] N. Stolterfoht, A. Arnau, M. Grether, R. Köhrbrück, A. Spieler, R. Page, A. Saal, J. Thomaschewski, and J. Bleck-Neuhaus, Phys. Rev. A **52**, 445 (1995).